APOLLO: Multiplexed Lunar Laser Ranging

T. W. Murphy, Jr., E. G. Adelberger, J. D. Strasburg, & C. W. Stubbs

Dept. of Physics, University of Washington, Seattle, WA 98195-1560

Abstract

The Apache Point Observatory Lunar Laser-ranging Operation (APOLLO) is a next-generation lunar laser ranging (LLR) campaign aimed at order-of-magnitude improvements in tests of gravitational physics via millimeter range precision. We will employ the 3.5 m telescope at the Apache Point Observatory (APO), located in southern New Mexico at an altitude of 2800 m. As a result of the large aperture size and excellent seeing conditions at the site, APOLLO expects to detect 2–10 lunar return photons per pulse. Relative background immunity permits operation in daylight and at full moon, resulting in better sampling of the lunar orbit.

We will use avalanche photodiode (APD) arrays as the detector for APOLLO, allowing multiple photons within a single return pulse to be individually time-tagged with high precision. Immediate advantages are shot-by-shot range profiles, as well as guaranteed calibration for each shot. In conjunction with a high time-precision start photodiode, one quickly builds an accurate representation of the convolved laser-detector-electronics temporal response. We describe here the hierarchical, multiplexed APOLLO timing system and its implementation using commercial electronics and a programmable logic controller. We also discuss the various calibration procedures geared toward millimeter precision. There is no practical limit to the number of channels employed in our timing scheme, allowing an upgrade path to larger APD array formats (10×10 or larger) in the future.

1 Introduction

Lunar laser ranging (LLR) has provided a laboratory for tests of fundamental physics for over three decades [1, 2]. Centimeter-precision range information provides measurements at the part in 10^{13} level by comparison to solar-system-scale phenomena. As we build the lunar-range database, some measurements become increasingly sensitive with the passage of time even without improvements in the range precision. For example, sensitivity to the time variation of Newton's gravitational constant, G, improves as the square of the observation time—now constrained at the impressive level of less than a part per trillion change per year [3].

While LLR may still deliver improved tests of physics in the years to come, the potential for order-of-magnitude improvements is best enabled by a new campaign intent on making order-of-magnitude improvements to the range precision itself. Current systems deliver range normal-points with typical uncertainties around 2 cm [4]. The greatest impediment to substantial improvement in range precision is photon number. Because the strength of the return signal from a passive reflector varies as the inverse fourth-power of distance, laser ranging to the moon is at the very limit of detectability. For example, the McDonald Laser Ranging Station (MLRS, [5]) at its very best detects just over one photon per minute (600 laser shots), placing about 15 photons into one normal point. From a purely statistical standpoint, order-of-magnitude range improvements would necessitate ~ 1500 photons per normal point—well beyond the capabilities of current LLR stations.

By establishing lunar range capability on the 3.5 m telescope at the Apache Point Observatory, we anticipate moving into the multiple-photon-per-pulse regime [6]. At a 20 Hz pulse repetition rate, the requisite photon number is accumulated in a matter of minutes. However, the high photon return rate presents instrumental challenges if one is to measure the lunar distance in an unbiased way. In particular, a signal consisting of a few photons is not large enough to reliably define a pulse shape on which one could perform a meaningful centroid or leading-edge measurement. Nor is this signal strength suitable for single-photon detectors such as avalanche photodiodes (APDs), which ignore all but the first detected photon. We will describe here the technique adopted for APOLLO to perform an unbiased measurement on a pulse containing a small number of photons. This paper will largely concentrate on the timing scheme employed to accommodate an arbitrary number of single-photon detector channels, which for APOLLO assumes the form of an APD array.

APOLLO expects to deliver range precision in the neighborhood of one millimeter. This high level of precision will undoubtedly expose many model deficiencies, almost all of which will be associated with earth deformations and atmospheric influence. Even before the model has time to catch up to APOLLO's precision, we will be able to extract gravitational physics measurements out of the dataset, since these appear at very well-defined frequencies, unlikely to be mimicked by aperiodic backgrounds or by periodic influences at different frequencies. Within the course of several years, APOLLO will produce order-of-magnitude improvements in fundamental physics parameters. Specifically, APOLLO will provide the very best tests of the following aspects of gravity, to the precisions indicated:

- Test of the strong equivalence principle to 3×10^{-5}
- Test of the weak equivalence principle with $\Delta a/a \approx 10^{-14}$
- Measurement of $\dot{G}/G$ to 10^{-13} yr^{-1}
- Test of the $1/r^2$ law at the lunar distance scale to $\sim 10^{-12}$
- Measurement of geodetic (de Sitter-Fokker) precession to $\sim 3 \times 10^{-4}$

The test of the strong equivalence principle tests how gravitational energy itself gravitates—a crucial nonlinearity predicted by general relativity [7, 8, 9]. The weak equivalence principle probes compositional differences in the accelerations of two bodies, and will exceed laboratory tests of the same [10]. Characterization of $\dot{G}$ addresses the evolution of fundamental coupling constants against the backdrop of the expanding universe [11, e.g.]. The test of the inverse square law searches for new long-range forces, and may be able to subject certain brane-world cosmological scenarios to critical tests [12, 13]. Measurement of relativistic geodetic precession provides a measure of the curvature of local spacetime, and the effect this has on the orientation of coordinate systems [14].

In addition to the aformentioned gravitational measurements, APOLLO will deliver order-of-magnitude gains in lunar science, geodesy, coordinate determinations, etc. Especially improved will be lunar science, because the high photon return rate will enable range measurements to the complete set of lunar reflectors during each observation. Thus the lunar orientation and deformation will be very precisely determined.

2 APOLLO Photon Rate

The high photon rate expected from APOLLO is the key to achieving substantial gains in precision. The principal factors enabling APOLLO to accomplish its millimeter goal are the large telescope aperture and the excellent atmospheric seeing experienced at the site. The median net image quality of the APO 3.5 m telescope for long exposures is 1.05 arcseconds. A crude scaling of APOLLO to OCA (Observatoire de la Côte d'Azur: 1.5 m, 2.5 arcsecond image quality [15]) and MLRS (0.78 m, 4 arcsecond image quality [5]) indicates a signal gain of 35 and 300, respectively. A gain of this magnitude (roughly 10^2) is necessary for a single order-of-magnitude improvement in random range uncertainty.

A bottom-up calculation of the expected photon return rate based on the familiar link efficiency equation is also illuminating. For APOLLO's parameters, we calculate the following number of return photons per laser pulse:

$$N_{\mathrm{det}} = 5.4 \times \left(\frac{E}{115\,\mathrm{mJ}}\right)\left(\frac{\eta}{0.4}\right)^2\left(\frac{f}{0.25}\right)\left(\frac{Q}{0.3}\right)\left(\frac{n}{100}\right)\left(\frac{1\,\mathrm{asec}}{\Phi}\right)^2\left(\frac{10\,\mathrm{asec}}{\phi}\right)^2\left(\frac{\langle r\rangle}{r}\right)^4 \text{ photons.}$$

Here, E is the pulse energy, η is the one-way optical efficiency, f is the receiver throughput (dominated by narrow-band filter), and Q is the detector efficiency. We assume one arcsecond seeing, pointing toward the smaller of the Apollo arrays (100 array elements), 10 arcsecond divergence out of the corner cubes, and the moon at its mean distance. We have been intentionally pessimistic with regard to optical efficiencies, but nonetheless calculate a detection rate of 5 photons per pulse. This return rate exceeds that routinely experienced at OCA and MLRS by a factor of roughly 1000—at odds with the simpler scaling in the previous paragraph.

Although the link efficiency equation as applied to current LLR stations yields photon rates roughly an order-of-magnitude too optimistic for current LLR stations, this is not the case when applied to the LLR system that once operated on the 2.7 m telescope at McDonald Observatory. At roughly 0.8 photons per pulse, this system had a high enough photon return rate to enable real-time optimization of the system [16]. APOLLO will likewise operate in this regime. Even a factor of 100 degradation in efficiency (due to pointing, focus, etc.) will produce one photon per second—enough to attempt real-time adjustment of pointing, focus, transmit/receive misalignment, and beam collimation. All of these adjustments are actuated in APOLLO, allowing an automated optimization routine to find the parameters that yield peak performance.

Another indication that this expectation may be reasonable comes from the best historical performance of the MLRS and OCA LLR stations. Without the ability to fine-tune performance in a closed-loop, algorithmic manner, the idealized system capabilities are perhaps best characterized by the lucky occasions when the systems happened to be tuned to optimum performance. MLRS, for instance, reports receiving 120 photons in 41 minutes on the Apollo 15 reflector [17]. Considering the time spent steering the telescope, one might estimate a peak instantaneous rate of one photon every 10 seconds, or 0.01 photons per pulse. For OCA, a return rate of 0.1 photons per pulse was obtained on the Apollo 15 reflector [18]. Blindly scaling these rates by the factors computed above based on aperture and seeing alone, one predicts a peak photon rate for APOLLO of about 3 photons per pulse.

So far, the issue of background noise has been left out of the discussion, but here too APOLLO enters a new regime—owing largely to the very small accepted field of view of 1.2 arcsec. Because of this, APOLLO will be able to operate in full moon or daylight conditions without significant noise contamination. We predict about 0.2 photons per pulse per 100 ns gate, on the full moon.

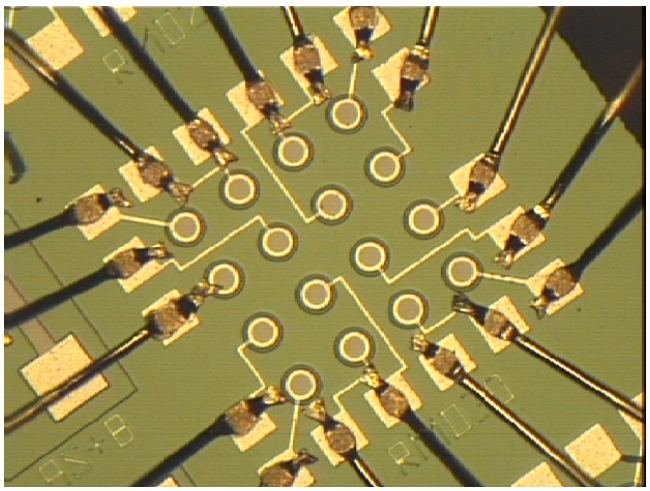

Figure 1: The 4×4 APD array APOLLO will use, courtesy of Lincoln Labs. The array elements are 30 μm in diameter, separated by 100 μm. Spatial information is preserved in the pixelated grid, and may be used to perform real-time guiding on the return signal.

Within the ~ 1 ns spread of lunar photon returns, our signal-to-noise ratio is ~ 500 with a signal return as low as one photon per pulse.

3 Array Detector

Traditionally, laser ranging (e.g., to satellites) has operated in either the single-photon mode—relying on the assumption that "double" photons are rare—or in large-signal mode, whereby the pulse shape is represented directly in the detector response. For our intermediate photon rate, neither is particularly suitable. Ideally, we would like to time-tag each detected photon individually. A single detector is incapable of this, because the detector response time is longer than the duration of the photon bundle. A multiplexed scheme is called for. One technique would string many single-element detectors along a chain of beam-splitters, such that each detector statistically receives some fraction of the incident light. Another technique is to use an array detector, spreading the return light spatially across the array such that any given element is again statistically likely to receive some fraction of the input light.

In collaboration with MIT Lincoln Laboratories, we have access to the APD array technology developed there. By fabricating APD structures into a monolithic silicon substrate, they have produced 4×4 and 32×32 array formats (see Figure 1). The elements have active areas of 20, 30, or 40 microns, placed on a square array pattern with 100 μm spacing. Details about the detector arrays may be found elsewhere [19].

The APD array that will initially be used in APOLLO is a 4×4 format with 30 μm elements (Figure 1). Because we want each of the elements to operate in single-photon mode (or an approximation to this), we want the likelihood of photon detection per element to be < 0.25, or about 4 photons across the array per pulse. At this upper limit, 25% of the detections will statistically be "double" detections, and a substantial bias correction must be applied—less for weaker returns. It has yet to be determined how high this upper limit should be for recovery of millimeter net accuracy in locating the geometrical center of the retroreflector array palette. The "comfort-zone" for an array of this size is around 1–3 photons per pulse, right where APOLLO expects to operate.

4 Multi-photon Calibration

The technique of measuring the time of departure of the outgoing laser pulse through the use of a corner-cube or other reflector in the telescope exit aperture is here called *calibration*. Serving as a time fiducial, this internal "return" allows one to make a *differential* measurement of target range by referencing the target return time to that of the corner-cube return. If measured in the same way as the target return, the calibration return eliminates systematic errors that are common to both paths.

Because it is necessary to measure both signals in the same manner, the calibration return must be attenuated to the level of the target return—down to the few-photon level. Here, the multiplexed approach offers a benefit over single-photon mode in that one may tune the calibration signal to generate several detected photons per pulse, and in doing so greatly reduce the number of pulses that have no fiducial reference. For example, if the system is operating at the 0.1 photon-per-pulse level, and the calibration is tuned to the same, only about 1% of the target returns will by chance have a calibration return associated with the same pulse. On the other hand, if the system is operating at N photons-per-pulse, the likelihood of detecting *no* calibration photons in a given pulse is e^{-N}, or less than 5% for $N = 3$. Thus one achieves greater assurance that each return shot has a fiducial time against which to compare.

Complete reliance on the calibration pulse to compute the round-trip travel time $\Delta t = t_{\text{target}} - t_{\text{cal}}$ would tend to produce uncertainties that are $\sqrt{2}$ times worse than the uncertainty of the target or calibration measurements separately. One can improve on this by also measuring the laser fire time using a fast photodiode and a constant-fraction discriminator to obtain a high signal-to-noise ratio estimate of the laser pulse time [21]. Comparison of the photodiode start with the target return does not qualify as a differential measurement, since the two are measured in wholly different ways. But one may nonetheless reference the calibration-return-time to the laser-fire-time, using the laser fire as a precision "*anchor*". The interval between the time anchor and the calibration return may vary as environmental conditions change—such as optical paths, cable delays, and electronics responses. But these changes are likely to be slow, with timescales of several minutes or more.

Under the assumption that the anchor drifts slowly, over short timescales one may reference the time of each calibration photon to this temporary fiducial. In this way, even calibration returns of only one photon may be properly placed with respect to the departure time of the center of the pulse. Figure 2 demonstrates this concept. At top is the system response—a convolution of laser pulse shape, detector jitter, electronics jitter, etc. This represents the distribution one would see emerge after a large number of photon events were recorded. The yellow vertical line indicates the centroid of the distribution. The rising edge of the laser pulse is detected by the fast photodiode, represented here as a thick green line. The placement is misleading since the calibration return arrives long after the photodiode trigger. But in a gedanken manner, one can simply delay the photodiode report until its relative position is as shown here.

Note that the single-shot mean, shown as vertical pink bars in Figure 2, "jumps" around by $\sim \sigma/\sqrt{N}$, where σ is the standard deviation of the convolved instrument response, and N is the number of photons in a given shot. The photodiode anchor eliminates this noise source, placing the photon events in their proper places (e.g., shots 3 and 11). Over five minutes, operating at 20 Hz and 2.5 photons per pulse, 15,000 calibration photon events are recorded. Thus one may build up an accumulated system response distribution with many events per time bin, approaching the black curve at the top of the figure. This distribution will differ from the target return by the small contribution from the fast photodiode jitter, and the generally larger contribution

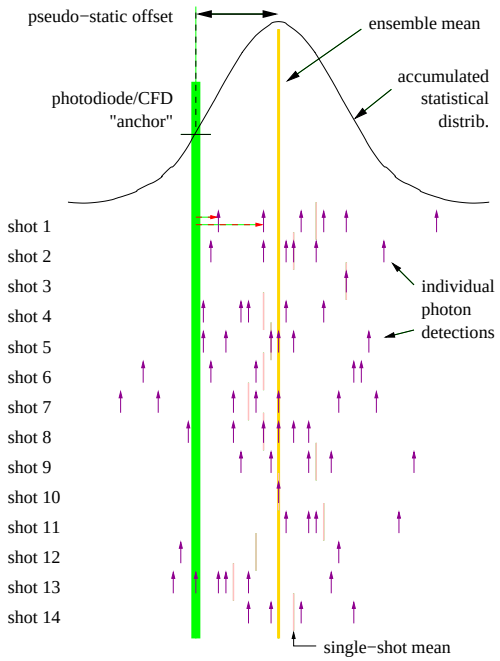

Figure 2: The multi-photon calibration scheme. Fourteen representative shots are displayed at an average rate of 4.5 photons per shot. Arrows represent individual photons. The vertical pink lines are the means within a shot. The thick green line is the high-precision photodiode start time. The profile at top and the vertical yellow line represent the accumulated properties of the photon time distribution.

from the target signature. Because the former is small, the latter may be directly determined by deconvolving the target response profile by the calibration response profile, provided that multi-photon biases have been properly treated.

In practice, once the offset between the photodiode anchor and the short timescale calibration ensemble mean (labeled as the pseudo-static offset in Figure 2) is determined, the time of arrival of target return photons may be directly referenced to the high-precision photodiode anchor time for that particular shot. The offset can be established based on a sliding averaging time—e.g., a time window of ±2 minutes about the current time. The character of the offset may be studied to determine appropriate timescales over which the assumption of slow changes holds, and as a tool for evaluating sources of systematic error.

5 Multiplexed Timing Scheme

A key ingredient of the APOLLO timing scheme is a 16-channel time-to-digital converter (TDC) made by Phillips Scientific (model 7186H [22]). At its highest resolution, the TDC measures intervals between 0–100 ns, at 12-bit (25 ps) resolution. Our tests show that its RMS jitter is around 13 ps per event. The TDC is responsible for measuring the time between photon arrival and a fiducial time mark derived from a precision oscillator. Figure 3 shows the general idea. At some time, in reference to the clock pulse train, the APD is turned (gated) on, after which photons may trigger detection events, and send START pulses to individual TDC channels. Figure 3 schematically displays six APD channels operating independently. Among the events depicted are four events clustered in a return packet, one sporadic background event, and one

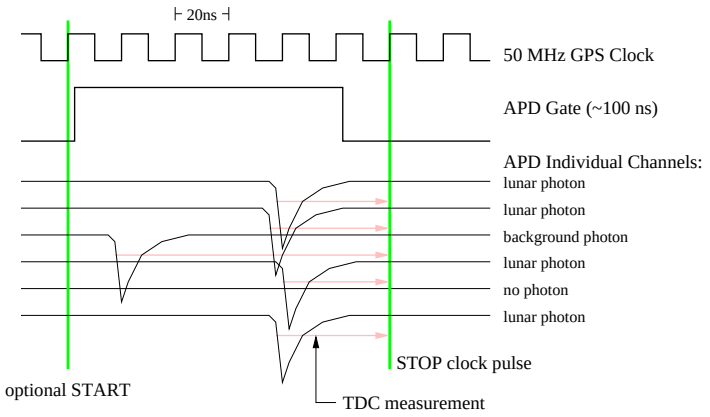

Figure 3: Schematic timing scheme. Photon events may occur within the APD gate, which is referenced to the 50 MHz clock. The time between the photon events and a selected clock pulse after the gate is measured for each channel by the TDC (pink arrow).

channel for which no photons were detected while the gate was on. After the gate is turned off, the next rising edge of the clock serves as a common STOP pulse to the TDC. Thus each TDC channel measures the interval between the photon event and this fiducial stop time.

Now if we simply know *which* clock pulse acted as the STOP, and the associated time, we then have all we need to measure the time between pulse departure and pulse return: $\Delta t = t_{\mathrm{STOP2}} - \Delta t_{\mathrm{TDC2}} - t_{\mathrm{STOP1}} + \Delta t_{\mathrm{TDC1}} + t_{\mathrm{offset}}$. The clock pulses may be counted continuously, and the counters latched on STOP events for readout. Reseting the counter once per second then ascribes more meaning to the count value: the time within the second. If the one pulse-per-second signal is derived from a clock synchronized to UTC, then the time of photon arrival may be determined to an accuracy of $\sim$ 50 ns (GPS$-$UTC accuracy), and a relative precision of $\sim$ 35 ps (dominated by the APD).

This is essentially the hierarchical scheme employed in APOLLO, composed of three pieces: clock time in seconds, pulse number in 20 ns intervals, and TDC measurement to 25 ps resolution. We additionally must predict the appropriate time to turn on the APD so that we catch the lunar return. A block diagram of the digital timing scheme appears in Figure 4. Each of the large boxes is clocked by a 50 MHz digital clock signal. The *gate width control* and the *target delay counter* are each counter/comparator schemes that send out a 20 ns pulse (CLOSE and target START, respectively) when some prescribed count is reached. For example, the counter in the *gate width control* is reset at either photodiode or target START signals, and counts in 20 ns intervals (corresponding to the 50 MHz clock) until the prescribed value, say 5, is reached. At that time, the APD gate is commanded to CLOSE, having been OPENed by the START pulse. The *target delay counter* is never reset, and has a wrap period of 5.4 seconds. At a gate CLOSE event, the counter value is latched and its data made available to the controlling computer. In the case of a calibration gate event—the one associated with laser fire—the target delay for that pulse is computed and fed via a first-in-first-out (FIFO) queue back into the *target delay counter*. When the free-running 50 MHz counter reaches this count, a target START event is generated.

Also shown are a few time-keeping blocks: the *counts-per-second* (CPS) block, and the *time-within-second* (TWS) block. The TWS counter is clocked at 50 MHz, and reset on the rising edge of the one pulse-per-second (1_PPS) signal from the GPS clock (TrueTime XL-DC). Because the 1 PPS signal is derived from the 50 MHz GPS signal, these two are co-phased. By latching the

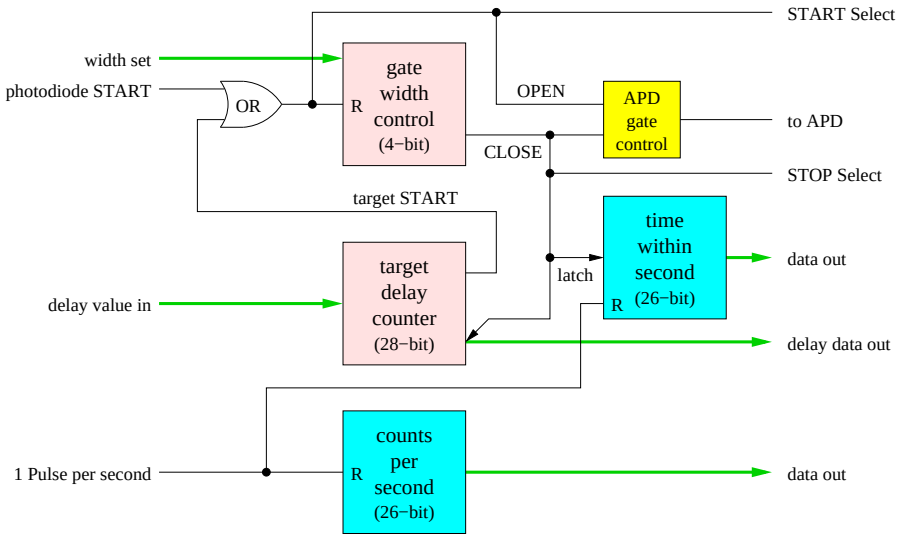

Figure 4: Block diagram of the APOLLO timing scheme. All blocks are clocked at 50 MHz.

value of the TWS counter at a CLOSE event, the exact clock pulse associated with the CLOSE event is unambiguously identified. Thus the time of the gate event within the GPS-clock-defined second is identified. The free-running counter, also latched by the CLOSE event, serves as a redundant check of the clock pulse number associated with the gate event. The CPS counter is another redundancy to verify proper counting of all clock pulses. Both latched and reset on the 1 PPS signal, this counter should always read 50,000,000 (minus two, as implemented).

The CLOSE and START signals perform another critical role in addition to the APD gate control. These 20 ns logic pulses are used to enable comparators whose input is the raw 50 MHz sine wave from the GPS clock. By bracketing a single positive voltage-swing of the sine wave with the 20 ns enable pulse, we can send a single clock pulse out of the comparator and to the TDC. In this way, the CLOSE signal slices a chosen clock pulse to act as a STOP, and optionally, the OPEN signal selects a START for the TDC. This latter capability allows us to send a START/STOP pair to the TDC whose time separation is a precise multiple 20.0 ns—depending on selected gate width—uncertain at the 10 ps level. The START pulse is simultaneously applied to all 16 input channels of the TDC, by way of the TEST input. In this way, we can calibrate each channel of the TDC against an absolute standard. At a data rate of 1 kHz, one may perform a sweep of the TDC at 20, 40, 60, 80, and 100 ns intervals in less than ten seconds, accumulating more than a thousand data points per interval. Rapid and frequent calibration will aid in the understanding and elimination of systematic errors.

The logic block of Figure 4 also shows various data paths. The inputs are used to set the width of the gate and the count associated with the next target event. The outputs pass the latched counter values. A computer controls this information exchange, recording data and calculating new target delay values.

This general timing scheme relies on multiplexing capability only in the TDC unit. The number of channels employed is irrelevant (until data input/output operations become limiting). APOLLO can easily upgrade to larger detector formats simply by employing additional TDC units.

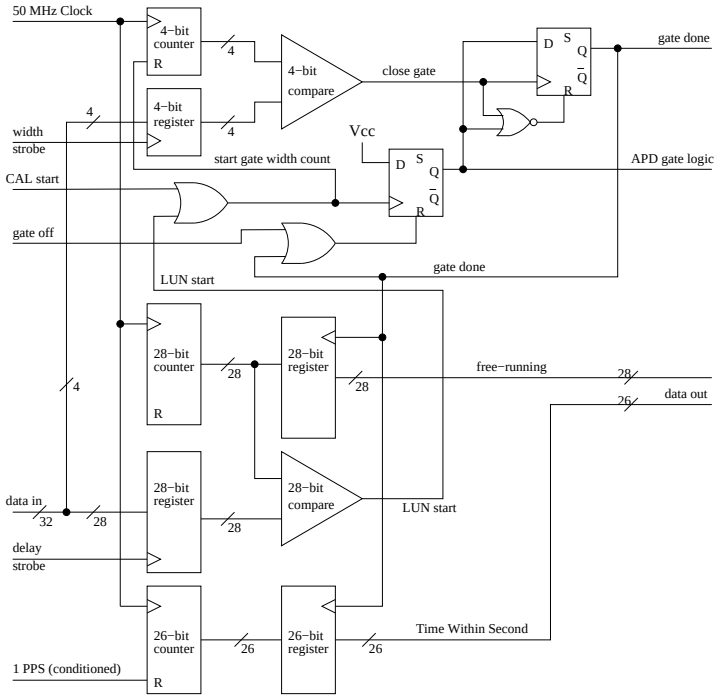

Figure 5: Approximate logic function of the main portion of the TIMER chip. Counters clocked at 50 MHz trigger events when their counts reach the values set in the adjacent registers. At top left is the gate width control, at top right is the APD gate control, at left center is the target delay generator, and at lower left is the time-within-second recorder.

6 Implementation: The APOLLO Command Module

The digital logic associated with the APOLLO timing scheme has been implemented on a custom CAMAC module called the APOLLO Command Module (ACM). The ACM is little more than two Altera programmable chips (MAX-7000AE series) interfacing to the CAMAC dataway and to various external hardware. The TIMER chip performs the timing logic, and contains the elements schematically depicted in Figure 4. The CAMAC chip controls the CAMAC interface, parsing commands, passing data, and setting the operating state of the TIMER chip. The chips are re-programmable in situ up to 1000 times. Thus the details of the logic functions may be changed via software, without needing access to the hardware.

A schematic example of the core elements in the TIMER chip (those represented in block form in Figure 4) is shown in Figure 5, though the details of the real implementation differ. The function of the ACM extends beyond that of counting clock pulses and controlling the APD gate. In total, the ACM performs the following tasks:

- keeping track of time (counting clock pulses and registering significant epochs),
- opening the APD gate in anticipation of photon arrival,
- controlling the duration of the APD gate,
- firing the laser in synchronization with the rotating transmit/receive switch,
- telling the 50 MHz stage when to send a STOP pulse to the TDC,

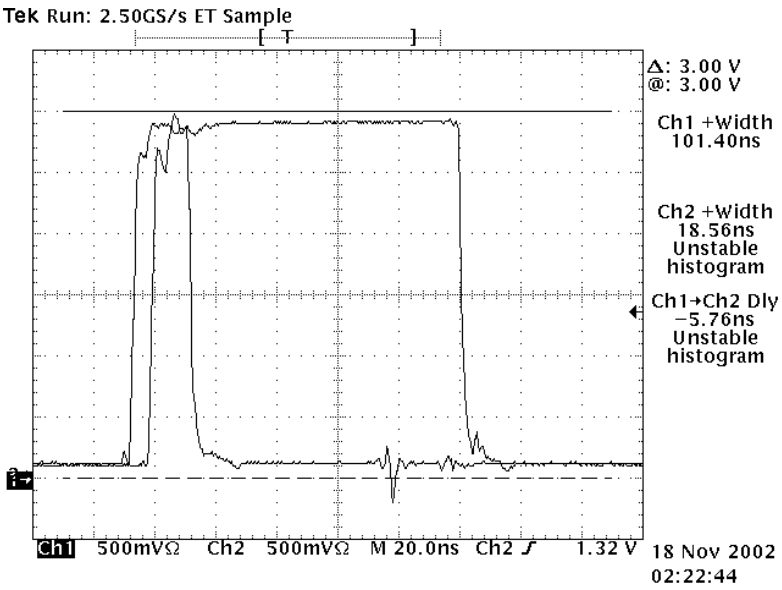

Figure 6: Oscilloscope trace of the ACM output, showing the OPEN signal and the GATE signal, about 6 ns later. The crossing at top is confusing, but the OPEN pulse is the shorter (20 ns) pulse that rises first.

- sending a time request to the GPS clock once per second,
- controlling entry into "stare" mode, allowing the APD to sense stars,
- blocking the laser when safety demands,
- and calibrating the TDC with pulses separated by precise multiples of 20.00 ns.

In addition, the ACM has safety features built in to prevent accidental damage to the APD or laser. There are also five as-yet unassigned ports, configurable as input or output, that may be used for future purposes. Potential uses include deploying corner cubes, setting the state of variable attenuators, etc.

The CAMAC communication rate is relatively high-speed, with a typical command duration of 1.5–2.0 μs. Test trials of the ACM controlled from a Linux machine running the stock RedHat 7.1 kernel (2.4.7) showed that the computer was able to keep up with the data rate (about 12 CAMAC commands per cycle) with no dropouts at rates of 300 Hz. Data dropouts were less than 0.5% up to about 20 kHz, becoming 50% at $\sim$ 40 kHz. It is at this point that the duration of the CAMAC command sequence—mostly reading data from the TIMER chip—exceeds the cycle time. These tests are somewhat unrealistic for the final control loop, because the roughly 20 commands necessary to read and reset all TDC channels were not included. Nonetheless, this scheme is capable of operation at several kHz in a practical ranging application. The few dropouts that do occur can be eliminated or reduced by applying low-latency patches to the Linux kernel, or by running Real-Time Linux, or some other low-latency operating system.

Figure 6 shows the appearance of ACM output pulses. In particular, the APD gate and the OPEN request pulses are shown. Each is a multiple of 20 ns in duration. The OPEN request is generated by the *target delay counter*, shortly followed by the gate pulse.

A picture of the "business end" of the ACM is shown in Figure 7. The CAMAC card-edge connector and input/output buffers are left out of this picture at bottom. At upper left is the

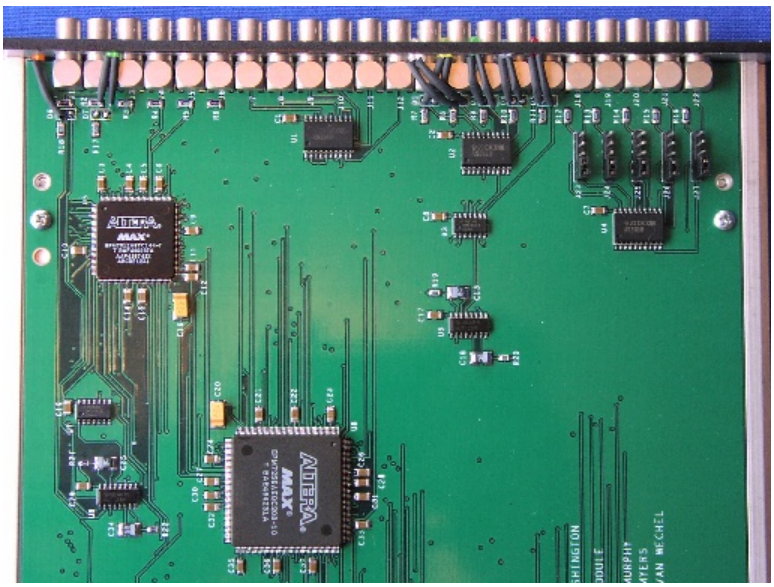

Figure 7: The APOLLO Command Module, showing the Altera programmable chips, and the many input/output connectors.

TIMER chip, with 10,000 gates, 512 macrocells, and 7 ns propagation delay. At bottom is the CAMAC chip, with 5,000 gates, 256 macrocells, and 10 ns propagation delay. Along the top, one can see the row of 22 LEMO-style connectors for interface to the rest of the system. The rightmost five connectors are jumper-configurable to act as outputs from or inputs to the TIMER chip.

The central role that the ACM plays in the APOLLO scheme may be appreciated by examination of Figure 8, showing the total APOLLO electronics system. The number of lines flowing into and out of the ACM—also evident from the number of connectors in Figure 7—would lead any physiologist to conclude that this must be the heart of the system. Another key interface is provided by the "booster stage," which multiplies the 10 MHz signal from the GPS clock by five, processes the selection of START and STOP pulses, and converts the NIM signal from the photodiode discriminator to an ECL (emitter-coupled logic) signal for the TDC.

7 Project Status

The color-coding of Figure 8 serves to show the status of integration of the APOLLO system. Most of the core system is in place. The ACM, having recently been completed, is undergoing initial testing. The APD circuitry is still in active development, and will likely continue to evolve up to the point of installation. Some of the peripheral equipment that is not yet needed has not yet been explored/selected.

The APDs have been tested, and we have concluded that their intrinsic jitter is in the neighborhood of 30 ps (see [19]). The APOLLO error budget therefore looks very promising, as summarized in Table 1. The single-photon RMS of the APOLLO system is around 8 mm, so that 1 mm precision may be statistically achieved in < 100 photons. Of course, the lunar reflector arrays introduce a large statistical spread depending on orientation, such that our photon requirement becomes roughly 1000 per normal point. If we detect one photon per pulse at 20 Hz, we will achieve this goal in less than one minute. In practice, five minutes per reflector is likely

Table 1: APOLLO Error Budget

Statistical Error Source	RMS Error (ps)	One-way Error (mm)
Laser Pulse (95 ps FWHM)	40	6
APD Jitter	30	4.5
TDC Jitter	15	2.2
50 MHz Freq. Reference	7	1
APOLLO System Total	52	8
Lunar Retroreflector Array	80–230	12–35
Total Error per Photon	100–240	14–37

to be sufficient.

The laser [23] has been delivered to Apache Point, and awaits installation on the telescope. Because the laser will be mounted on the telescope in the cold ambient environment, we are currently spending our time developing the appropriate thermal protections—both to the laser and to the dome environment.

Much remains to do before we acquire our first lunar data. We are optimistic that 2003 will bring many happy returns. See the APOLLO website for updates on our status [24].

Acknowledgements

We thank Tim van Wechel for his substantial design work on the APOLLO Command Module, and Allan Myers for its excellent fabrication. We also thank the Center for Experimental Nuclear Physics and Astrophysics (CENPA) for their donation of resources. Jesse Angle and Dan Miller also contributed to the project during the last year. APOLLO is supported by a grant from NASA.

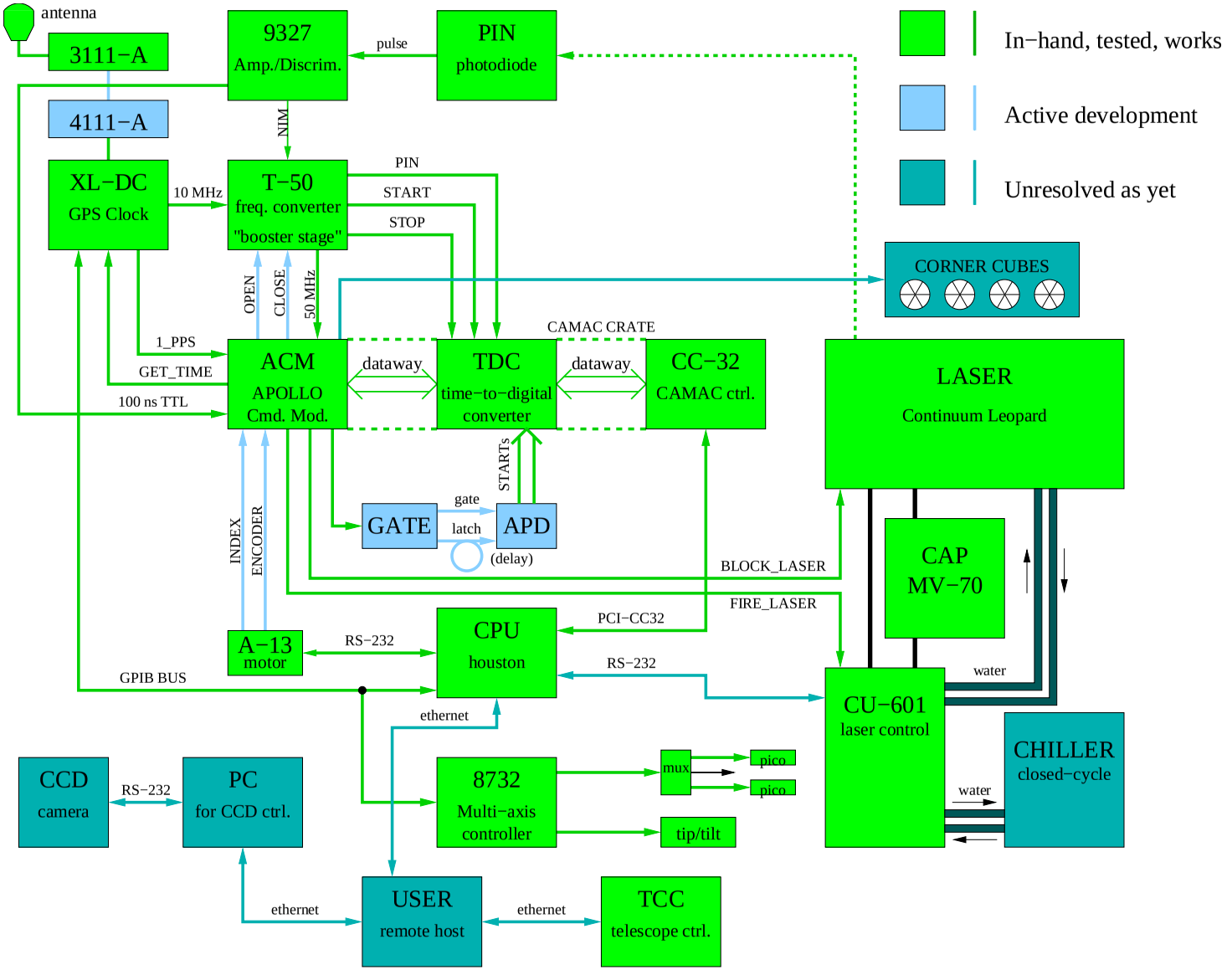

Figure 8: APOLLO block diagram showing the primary electronics components. Color-coding indicates current status.

References

[1] Bender, P. L., Currie, D. G., Dicke, R. H., Eckhardt, D. H., Fal ler, J. E., Kaula, W. M., Mullholland, J. D., Plotkin, H. H., Poultney, S. K., Silverberg, E. C., Wilkinson, D. T., Williams, J. G., & Alley, C. O., "The Lunar Laser Ranging Experiment," *Science*, **182**, 229, (1973)

[2] Dickey, J. O., Bender, P. L., Faller, J.E., Newhall, X. X., Rick lefs, R. L., Ries, J. G., Shelus, P. J., Veillet, C., Whipple, A. L., Wiant, J. R., Williams, J. G., & Yoder, C. F., "Lunar Laser Ranging: A Continuing Legacy of the Apollo Program," *Science*, **265**, 482, (1994)

[3] Williams, J. G., Boggs, D. H., Dickey, J. O., & Folkner, W. M., "Lunar Tests of the Gravitational Physics," *Proceedings of the Ninth Marcel Grossman Meeting*, Rome, Italy, June 2000, World Scientific Publications, R. Jantzen, ed., (2001)

[4] Anderson, J. D., & Williams, J. G., "Long-Range Tests of the Equivalence Principle," *Class. Quantum Grav.*, **18**, 2447, (2001)

[5] `http://almagest.as.utexas.edu/ rlr/mlrs.html`

[6] Murphy, T. W., Strasburg, J. D., Stubbs, C. W., Adelberger, E. G., Angle, J., Nordtvedt, K., Williams, J. G., Dickey, J. O., & Gillespie, B., "The Apache Point Observatory Lunar Laser-ranging Operation (APOLLO)," *12th International Laser Ranging Workshop*, Matera, Italy, (2000).

[7] Nordtvedt, K., "Equivalence Principle for Massive Bodies. I. Phenomenology," *Physical Review*, **169**, 1014, (1968)

[8] Nordtvedt, K., "Equivalence Principle for Massive Bodies. II. Theory," *Physical Review*, **169**, 1017, (1968)

[9] Damour, T., "Testing the equivalence principle: why and how?," *Class. Quantum Grav.*, **13**, A33, (1996)

[10] Baeßler, S., Heckel, B. R., Adelberger, E. G., Gundlach, J. H., Schmidt, U., & Swanson, H. E., "Improved Test of the Equivalence Principle for Gravitational Self-Energy," *Physical Review Letters*, **83**, 3585, (1999)

[11] Damour, T., & Nordtvedt, K., "Tensor-scalar cosmological models and their relaxation toward general relativity," *Phys. Rev. D*, **48**, 3436, (1993)

[12] Dvali, G., Gruzinov, A., & Zaldarriaga, M., "The Accelerated Universe and the Moon," LANL preprint archive, `xxx.lanl.gov/abs/hep-ph/0212069`, 5 Dec., (2002)

[13] Lue, A., & Starkman, G., "Gravitational Leakage into Extra Dimensions: Probing Dark Energy Using Local Gravity," LANL preprint archive, `xxx.lanl.gov/abs/astro-ph/0212083`, 11 Dec., (2002)

[14] Williams, J. G., Newhall, X. X., & Dickey, J. O., "Relativity parameters determined from lunar laser ranging," *Physical Review D*, **53**, 6730, (1996)

[15] Samain, E., Mangin, J. F., Veillet, C., Torre, J. M., Fridelence, P., et al., "Millimetric Lunar Laser Ranging at OCA (Observatoire de la Côte d'Azur," *Astronomy & Astrophysics Suppl. Ser.*, **130**, 235, (1998)

[16] Silverberg, E. C., private communiucation (2002)

[17] Wiant, J. R., private communiucation (2002)

[18] Samain, E., private communiucation (2002)

[19] Strasburg, J. D., et al., "The advantages of Avalanche Photodiode (APD) arrays in laser ranging applications," *13th International Laser Ranging Workshop*, Washington, D. C., USA, (2002).

[20] Nordtvedt, K., "Optimizing the observation schedule for tests of gravity in lunar laser ranging and similar experiments," *Classical Quantum Gravity*, **15**, 3363, (1998)

[21] Using Hamamatsu G4176 photodiode, Picosecond Pulse Labs Model 5545 bias tee, and Ortec 9327 amplifier/constant-fraction-discriminator.

[22] `http://www.phillipsscientific.com/phisci1.htm`

[23] `http://www.psplc.com/leopard.html`

[24] `http://www.astro.washington.edu/tmurphy/apollo/apollo.html`